Bulg. J. Phys. **44** (2017) 319–325

Bohr Model Solution for a Shape Coexisting Potential

R. Budaca, **P. Buganu**, **A.I. Budaca**
Horia Hulubei National Institute of Physics and Nuclear Engineering,
RO-077125 Bucharest-Magurele, Romania

Received *31 October 2017*

Abstract. The prolate version of the Bohr Hamiltonian with a potential having simultaneous spherical and deformed minima of the same depth is diagonalized in a basis defined through the Bessel-Fourier expansion method. When only $K = 0$ states are considered, the condition of degenerate minima restricts the model to a single free parameter connected to the height of the barrier which separates the two minima. Shape coexistence within the same collective state emerges for specific intervals of the free parameter when the state is in the vicinity of the barrier peak. The measure of mixing between the coexisting deformations is investigated by means of transition matrix elements relevant to electromagnetic observables.

PACS codes: 21.60.Ev, 21.10.Re, 27.70.+q

1 Introduction

In the framework of the Bohr-Mottelson (BM) model [1, 2], the critical point potential for the shape phase transition between spherical and axially deformed nuclear shapes has two degenerate minima, one spherical and another one deformed, separated by a small barrier. The transition from spherical to deformed shapes is realized by having the deformed minimum deeper than the spherical one. This kind of transition is said to be of the first order. A potential with degenerated minima is naturally supposed to describe two coexisting shapes [3]. Although, in the present conception of nuclear theory [4], shape coexistence is a general occurrence in nuclear systems, the term is however used when the coexistence is associated to very different deformation configurations such as prolate-oblate, deformed-spherical, or high-low deformation. Here, one will discus the conditions in which, a potential with double degenerated minima is indeed associated to shape coexistence and how one can detect such behaviour. To do this, one diagonalizes the prolate version of the Bohr Hamiltonian with a sextic potential in the β shape variable. The potential is restricted to have degenerated minima. The choice of diagonalization basis is inspired by the infinite square well

solutions associated to critical points of various shape phase transitions [5–11]. The common feature of these solutions is the satisfaction in various degrees of the Euclidean dynamical symmetry differential equation [11–16] which can be reduced to the Bessel equation. Therefore, the wave function for the present problem can be constructed through a Fourier-Bessel expansion [19–21].

In the following section, one will present the model Hamiltonian and the corresponding differential equations to be solved. After that, a brief description of the diagonalization method will be given. The numerical application of the model will be devoted to the discussion of particularities of the electromagnetic properties in the model's space where the shape coexistence features are emerging. The results will be summarized in the final section.

2 Theoretical Framework

By assuming a decoupling of the β and γ degrees of freedom in the Bohr Hamiltonian, which is customary for axially deformed nuclear shapes [6], one usually arrives to the following radial-like differential equation for the β shape variable

$$\left[-\frac{1}{\beta^4}\frac{\partial}{\partial\beta}\beta^4\frac{\partial}{\partial\beta}+\frac{L(L+1)}{3\beta^2}+v(\beta)\right]\Psi(\beta)=\epsilon^\beta\Psi(\beta)\,, \tag{1}$$

where B is the mass parameter, L is the angular momentum quantum number, while $v(\beta)$ is the separated β part of the total potential. The latter is considered to be a general sextic polynomial in β

$$v(\beta)=a\beta^2+b\beta^4+c\beta^6\,. \tag{2}$$

In this way, one can have double minima with the least number of terms. The Schrödinger equation for all polynomial potentials have useful scaling properties [17, 18, 22]. The same is true for the sextic potential wave equation, which is scaled as

$$\epsilon^\beta(a,b,c)=a^{1/2}\epsilon^\beta(1,ba^{-3/2},ca^{-2})\,. \tag{3}$$

Taking into account this property, the solution for the potential (2) is equivalent to that for the potential

$$v(\beta)=\beta^2+\mu\beta^4+\nu\beta^6\,, \tag{4}$$

which contains now only two parameters. The expression for this potential with an additional restriction to have two minima which are degenerated can be written as

$$v(\beta)=\beta^2-2q\beta^4+q^2\beta^6\,. \tag{5}$$

This potential has a single free parameter q. The spherical (s) and deformed (d) minima of this potential correspond to $v(\beta_s)=v(\beta_d)=0$ and are positioned

at $\beta_s = 0$ and respectively $\beta_d = 1/\sqrt{q}$. For a simplified and a more unified description of the differential equation for such a potential, it is useful to make the change of variable $y = \sqrt{q}\beta$. In this way, the differential equation (1) becomes

$$\left[-\frac{\partial^2}{\partial y^2} - \frac{4}{y}\frac{\partial}{\partial y} + \frac{L(L+1)}{3y^2} + v(y)\right]\Psi(y) = E\Psi(y)\,, \tag{6}$$

where

$$v(y) = \frac{1}{q^2}\left(y^2 - 2y^4 + y^6\right), \;\; E = \frac{\epsilon^\beta}{q}\,. \tag{7}$$

The advantages of this y-form are related to the constant position for the deformed minimum ($y_d = 1$) and the barrier peak ($y = 1/\sqrt{3}$). The only q-dependent quantities are now the height of the barrier which separates the two minima and the slope of the outer wall of the potential.

3 Diagonalization Procedure

The solutions of the Schrödinger equation (6) with the potential (7) are found by diagonalizing it within a basis constructed as a truncated Fourier-Bessel series [19–21] of the exact wave function. The basis states are defined as solutions for an infinite square well potential

$$\tilde{v}(y) = \begin{cases} 0, & y \le y_W\,, \\ \infty, & y > y_W\,, \end{cases} \tag{8}$$

with a carefully chosen position for the infinite wall y_W such that to encompass the oscillatory part of the original polynomial potential. These are proportional to bessel functions of the first kind

$$\tilde{\Psi}_{\nu n}(y) = \frac{\sqrt{2}y^{-\frac{3}{2}}J_\nu(\alpha_n y/y_W)}{y_W J_{\nu+1}(\alpha_n)}\,, \tag{9}$$

with

$$\nu = \sqrt{\frac{9}{4} + \frac{L(L+1)}{3}}\,. \tag{10}$$

The other index $n = 1, 2, 3...$ denotes the order of the Bessel function's zeros $\alpha_n = y_W\lambda$, and counts also the basis states.

Expanding the solution of equation (6) in the basis of the orthogonal functions (9)

$$\Psi_{Lk}(y) = \sum_n^{n_{max}} A_n^k \tilde{\Psi}_{\nu n}(y), \;\; k = 1, n_{\max} \tag{11}$$

and truncating the series at a finite dimension n_{max} one can determine the corresponding eigenvalues by diagonalizing the Hamiltonian matrix defined in

this truncated basis. The matrix elements of the Hamiltonian in the truncated Fourier-Bessel basis are calculated using the following expression:

$$H_{nm} = \frac{\alpha_n}{y_W}\delta_{nm} + \frac{2\sum_{i=1}^{3} v_i \left(y_W\right)^{2i} I_{nm}^{(\nu,i)}}{q^2 J_{\nu+1}(\alpha_n) J_{\nu+1}(\alpha_m)}\,, \tag{12}$$

where $v_1 = v_3 = 1$ and $v_2 = -2$ and

$$I_{nm}^{(\nu,i)} = \int_0^1 x^{2i+1} J_\nu(\alpha_n x) J_\nu(\alpha_m x) dx,\ x = y/y_W\,. \tag{13}$$

The set of final eigenvalues for a certain value of ν and implicitly a fixed angular momentum L are distributed to different β vibrational bands. More precisely, the lowest eigenvalue for a given angular momentum state is assigned to the ground band, the second lowest to the first excited β band and so on.

The basis is truncated at $n_{max} = 20$, which assures convergent eigenvalues for all considered states. The boundary limit associated to a chosen potential $v(y)$ is then fixed in such a way as to have a convergence accuracy $\varepsilon = 10^{-7}$ for the highest considered energy state of Eq.(6), which is set to be $(L = 20, n_\beta = 1)$. The convergence of lower states is then confirmed through numerical try-outs.

4 Numerical Application

The general characteristics of the model were addressed in Ref. [23]. Here we are concerned with the domain of q values which brings out features which are associated to shape coexistence. First of all, for the sake of clarity, one must make a comment on the types of shape coexistence. Suppose that we have two possible very different deformation configurations. If the two deformation states do not interact, then the shape coexistence will manifest itself through two non-interacting bands with different deformations which will compete to become the ground band. Whereas, if the two deformation configurations interact or mix, then one will have two energetically distinct bands whose states are superpositions of the two pure deformation states. In the latter case, one says that the shape coexistence is not only in the same nucleus, but also in the same state. In Ref. [23], it was shown that the double minima potential leads only to a shape coexistence of the second kind, and even that only in special circumstances. More precisely, the states become mixed or with clear sizable components of different deformation only in the vicinity of the barrier peak which separates the two deformation minima. The asymmetry or the splitting of the density probability distribution is a clear evidence of shape coexistence within a state. The best signature for such a shape coexistence is the abnormally high strengths of the monopole transitions between the states belonging to the two mixed bands [24]. In the framework of the present model, the monopole transition strength is proportional to the matrix element $\langle f|\beta^2|i\rangle^2 = \langle \Psi_f(y)|y^2/q|\Psi_i(y)\rangle^2$. This quantity has a maximum at $q = 0.0589$ for the transition connecting the ground state

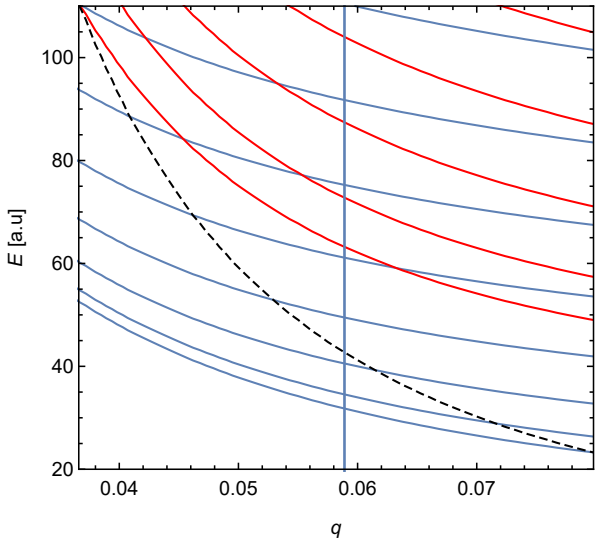

Figure 1. (color online) Absolute values of the ground band (blue lines) and β band (red lines) energy levels are given in arbitrary units as a function of the free parameter q. The interval of q values is chosen between the intersections of the dashed line representing the evolution of the barrier peak height with the β band-head state and respectively the ground state. The vertical line marks the $q = 0.0589$ value which maximizes the monopole strength.

and the β band-head state. This value is just between the situations where the barrier peak touches the β band-head ($q = 0.0366$) and respectively the ground state ($q = 0.0798$). The evolution of the relationship between the energy levels and the barrier peak is depicted in Figure 1.

As can be seen from Figure 1, when $q = 0.0589$, the height of the barrier is above and very close to the 4_g^+ state. It is interesting that the energy spectrum for this case do not present any particular behaviour. Indeed, the energy levels have a smooth evolution as function of q [23], including the interval of interest for shape coexistence visualized in Figure 1. As the energy levels do not give away any hint of shape coexistence, one turns once again our attention to electromagnetic properties which are directly related to the particularities of the deformation density probability distribution. The proximity of the barrier to the 4_g^+ state when q has the critical value of 0.0589, suggests that a transition probability connected to this state might provide some information regarding deformation configuration mixing. In Figure 2 we plotted the ratio $B(E2; 4_g^+ \rightarrow 2_g^+)/B(E2; 2_g^+ \rightarrow 0_g^+)$ as a function of q. The graphical representation is made for a complete range of q values, such that one can observe the reproduction of the rigid rotor (R.R.) and $X(5)$-β^6 [25] limits not only in respect to the energy spectrum [23] but also in the $E2$ transition probabilities. The

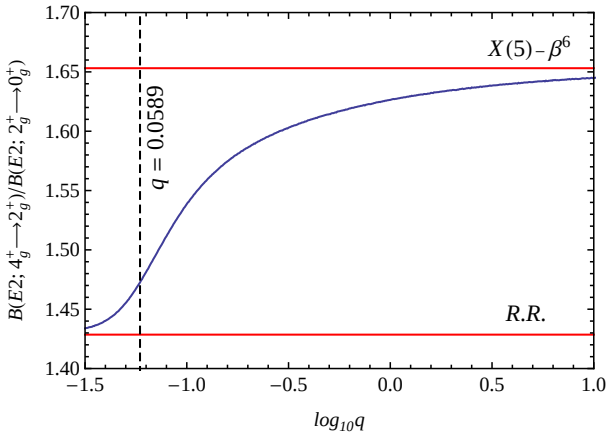

Figure 2. (color online) The ratio $B(E2;4_g^+ \rightarrow 2_g^+)/B(E2;2_g^+ \rightarrow 0_g^+)$ given as a function of $\log_{10} q$. The values corresponding to the rigid rotor estimation and that corresponding to the $X(5)$-β^6 prediction are presented as red lines for reference. The vertical dashed line marks the critical value of the transition between the rigid rotor picture and the critical point instance described by the $X(5)$-β^6 model.

transitional aspect [3] of the curve is quite obvious. Moreover, it happens that numerically the inflection point where the actual transition takes place is just in the critical value $q = 0.0589$. In this point, the second derivative of the transitions ratio changes signs. Because the transition takes place relatively abrupt, the ratio between the first $E2$ transitions from the ground band can be used to search critical point nuclei which exhibit also shape coexistence.

From the few numerical fits performed on actual nuclei in Ref. [23], ^{152}Nd nucleus emerges as a possible representative for the double fold critical point represented by the theoretical model in $q = 0.0589$.

5 Conclusions

The Bessel-Fourier expansion method was used to construct a basis for the diagonalization of a prolate version of a Bohr Hamiltonian with a sextic potential in the β shape variable with two degenerated minima, spherical and deformed. Due to the specific construction of the model and its scaling property, the spectrum and wave functions of the $K = 0$ bands depend on a single free parameter which is related to the height of the separating barrier. The dependence of the model on a single free parameter allowed a complete description of the transition from an $SU(3)$ behaviour of the nucleus to a critical point instance associated to a $X(5)$-type solution. Thus it was found that the emergence of coexisting shapes in low-lying states is conditioned by the proximity of these states to the peak of

the barrier. In conclusion, in certain conditions, the critical point of a first order shape phase transition can describe a shape coexisting situation. Moreover, the shape coexistence in the critical point of the shape phase transition between spherical and axially deformed nuclei is revealed by studying the electromagnetic properties rather than the energy spectrum.

Acknowledgments

Support from the CNCS-UEFISCDI, project number PN-III-P4-ID-PCE-2016-0092 is gratefully acknowledged.

References

[1] A. Bohr (1952) *Mat. Fys. Medd. K. Dan. Vidensk. Selsk.* **26** 14.
[2] A. Bohr and B.R. Mottelson (1953) *Mat. Fys. Medd. Dan. Vidensk. Selsk.* **27** 16.
[3] R.F. Casten (2006) *Nature Phys.* **2** 811.
[4] K. Heyde and J.L. Wood (2011) *Rev. Mod. Phys.* **83** 1467.
[5] F. Iachello (2000) *Phys. Rev. Lett.* **85** 3580.
[6] F. Iachello (2001) *Phys. Rev. Lett.* **87** 052502.
[7] D. Bonatsos, D. Lenis, D. Petrellis, and P.A. Terziev (2004) *Phys. Lett. B* **588** 172.
[8] D. Bonatsos, D. Lenis, D. Petrellis, P.A. Terziev, and I. Yigitoglu (2005) *Phys. Lett. B* **621** 102.
[9] D. Bonatsos, D. Lenis, D. Petrellis, P.A. Terziev, and I. Yigitoglu (2006) *Phys. Lett. B* **632** 238.
[10] R. Budaca and A.I. Budaca (2016) *Phys. Rev. C* **94** 054306.
[11] R. Budaca and A.I. Budaca (2016) *Phys. Lett. B* **759** 349.
[12] M.A. Caprio and F. Iachello (2007) *Nucl. Phys. A* **781** 26.
[13] D. Bonatsos, E.A. McCutchan, and R.F. Casten (2008) *Phys. Rev. Lett.* **101** 022501.
[14] D. Bonatsos, E.A. McCutchan, R.F. Casten, R. J. Casperson, V. Werner, and E. Williams (2009) *Phys. Rev. C* **80** 034311.
[15] Yu Zhang, Yu-Xin Liu, Feng Pan, Yang Sun, and J.P. Draayer (2014) *Phys. Lett. B* **732** 55.
[16] Yu Zhang, Feng Pan, Yu-xin Liu, Yan-An Luo, and J.P. Draayer (2014) *Phys. Rev. C* **90** 064318.
[17] R. Budaca (2014) *Eur. Phys. J. A* **50** 87.
[18] R. Budaca (2014) *Phys. Lett. B* **739** 56.
[19] H. Taşeli and A. Zafer (1997) *Int. J. Quant. Chem.* **61** 759.
[20] H. Taşeli and A. Zafer (1997) *Int. J. Quant. Chem.* **63** 935.
[21] H. Taşeli and A. Zafer (1998) *J. Comput. Appl. Math.* **95** 83.
[22] R. Budaca, P. Buganu, M. Chabab, A. Lahbas, and M. Oulne, *Ann. Phys. (NY)* (2016) **375** 65.
[23] R. Budaca, P. Buganu, and A.I. Budaca (2018) *Phys. Lett. B* **776** 26.
[24] J.L. Wood, E.F. Zganjar, C. De Coster, and K. Heyde (1999) *Nucl. Phys. A* **651** 323.
[25] D. Bonatsos, D. Lenis, N. Minkov, P.P. Raychev, P.A. Terziev, (2004) *Phys. Rev. C* **69** 014302.